Electronic Supplementary Information (ESI)

Highly-Integrated, Laser Manipulable Aqueous Metal Carbonyl Vesicles (MCsomes) with Aggregation-Induced Emission (AIE) and Aggregation-Enhanced IR Absorption (AEIRA)

Nimer Murshid,[a] Ken-ichi Yuyama,[b] San-Lien Wu,[b] Kuan-Yi Wu,[b] Hiroshi Masuhara,[b] Chien-Lung Wang[b] and Xiaosong Wang[*a]

[a] Department of Chemistry and Waterloo Institute for Nanotechnology, University of Waterloo, 200 University Avenue West, Waterloo, Ontario, N2L 3G1, Canada

[b] Department of Applied Chemistry and Institute of Molecular Science, National Chiao Tung University, Hsinchu 30010, Taiwan

Table of Contents

1. Principle of laser trapping

Laser trapping phenomenon for particles with the size much smaller than the wavelength of the trapping laser is conventionally interpreted by Maxwell Boltzmann electromagnetic theory. The gradient force exerted on nanometer-sized objects is given as follows:[1,2]

$$\mathbf{F}_{grad} = \frac{1}{2}\varepsilon_m \alpha \nabla \mathbf{E}^2 \qquad (1).$$

Here E denotes the electric field, and ∇ represents a gradient with respect to the spatial coordinates. The parameter of ε_m represents the permittivity of the surrounding medium. The polarizability of the nanoparticle, α, under the dipole approximation, is given by

$$\alpha = 4\pi r^3 \frac{\left(\dfrac{n_p}{n_m}\right)^2 - 1}{\left(\dfrac{n_p}{n_m}\right)^2 + 2} \qquad (2).$$

Notations of r, is the radius of the nanoparticle. n_p and n_m represent the refractive index of the nanoparticle and the surrounding medium, respectively. As calculated from above equations, no gradient force is given to a target nanometer-sized object in the case that its refractive index is the same as that of the surrounding medium. When the target object has the refractive index higher than that of the surrounding medium, the gradient force toward the focal spot is exerted on the object, and its magnitude becomes larger with the increase in the refractive index of the target object.

[1] Y. Harada, T. Asakura, *Opt. Commun.*, 1996, **124**, 529–541
[2] T. Sugiyama, K.-I. Yuyama, H. Masuhara, *Acc Chem Res*, 2012, **45**, 1946–1954

2. Quantum yield measurement

Quantum yield for the aqueous solution of **1** was compared with 1,4-bis(5-phenyloxazol-2-yl) benzene (POPOP) in cyclohexane as a reference. UV-vis spectra were measured for diluted solutions of POPOP in cyclohexane and colloid of **1** in water. Fluorescence spectra were then recorded for the same samples with excitation wavelength of 350 nm. The collected data was used to calculate the quantum yield of **1** using the following equation.[3]

$$Q = Q_R \times \frac{FL\ integration}{FL_R\ integration} \times \frac{1 - 10^{-A_R}}{1 - 10^{-A}} \times \frac{n^2}{n_R^2}$$

Q = Quantum yield for the sample

A = absorbance at excitation wavelength for the sample

n = refractive index of the solvent for the sample

FL integration = area under the emission spectra of the sample

Q_R = Quantum yield for the standard

A_R = absorbance at excitation wavelength for the standard

n_R = refractive index of the solvent for the standard

FL_R integration = area under the emission spectra of the standard

All samples were measured at the same time under same conditions. The florescence emission spectra were measured with excitation wavelength of 350 nm.

[3] A. M. Brouwer, *Pure Appl. Chem.*, 2011, **83**, 2213–2228

3. Synthesis and characterization of 1

As illustrated in Scheme S1, the building block (**1**) is prepared via a migration insertion reaction (MIR) of a bithiophene tethered Fp derivative (**2**) in the presence of triphenylphosphine. **2** is obtained from the reaction of **3** with FpK and **3** is prepared via the reaction of 5-lithio-2,2'-bithiophene with 1-bromo-3-chloropropane. ^{1}H NMR for **3** is illustrated in Figure S1. Fig. S2 display the ^{31}P NMR and IR spectra for **1**. As shown in the figure, only one signal in the ^{31}P NMR spectrum appears at 77.4 ppm due to the coordinated phosphorus element (Fig. S2a) and both terminal CO and acyl CO groups appear in the IR spectrum for **1** (Fig. S2b) at 1905 and 1600 cm^{-1}, respectively, suggesting that the migration insertion reaction has occurred.[4] In ^{1}H NMR spectrum, the down field signals appear at 7.37 – 7.49 ppm are due to the phenyl protons, while those between 6.55 and 7.15 ppm represent the protons from the bithiophene units. The downfield shift for signal due to the protons of Cp ring to 4.41 ppm and upfield shift of the two diastereotopic α-protons with splitting chemical shifts at 2.67 and 2.90 ppm (a in Fig. S2) suggest that the migration insertion reaction has occurred.[4] The detailed chemical shifts are summarized in the Experimental Section.

[4] X. Wang, K. Cao, Y. Liu, B. Tsang, S. Liew, *J. Am. Chem. Soc.*, 2013, **135**, 3399−3402

4. Supporting Figures and analysis
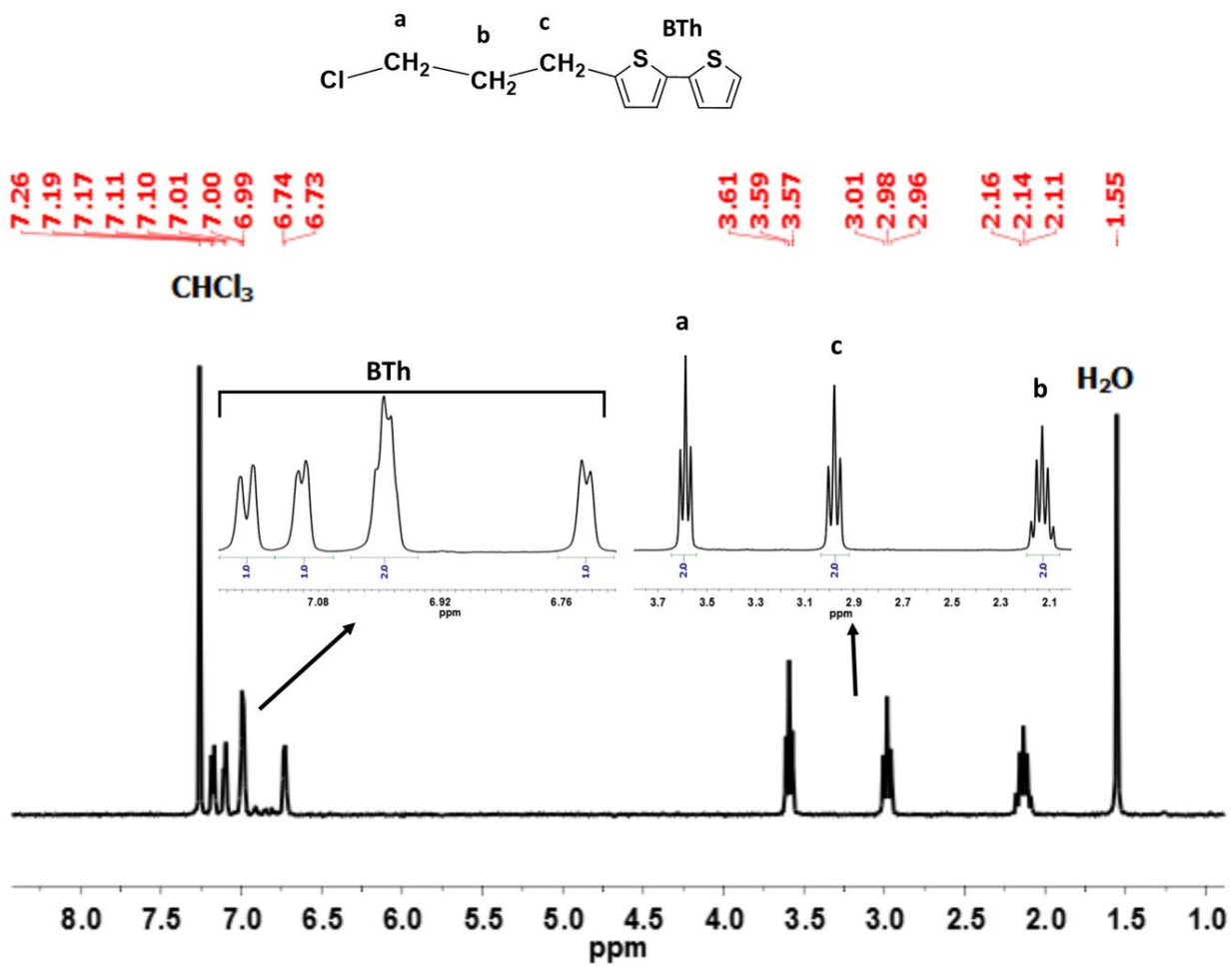
Scheme S1. Synthesis of **1**
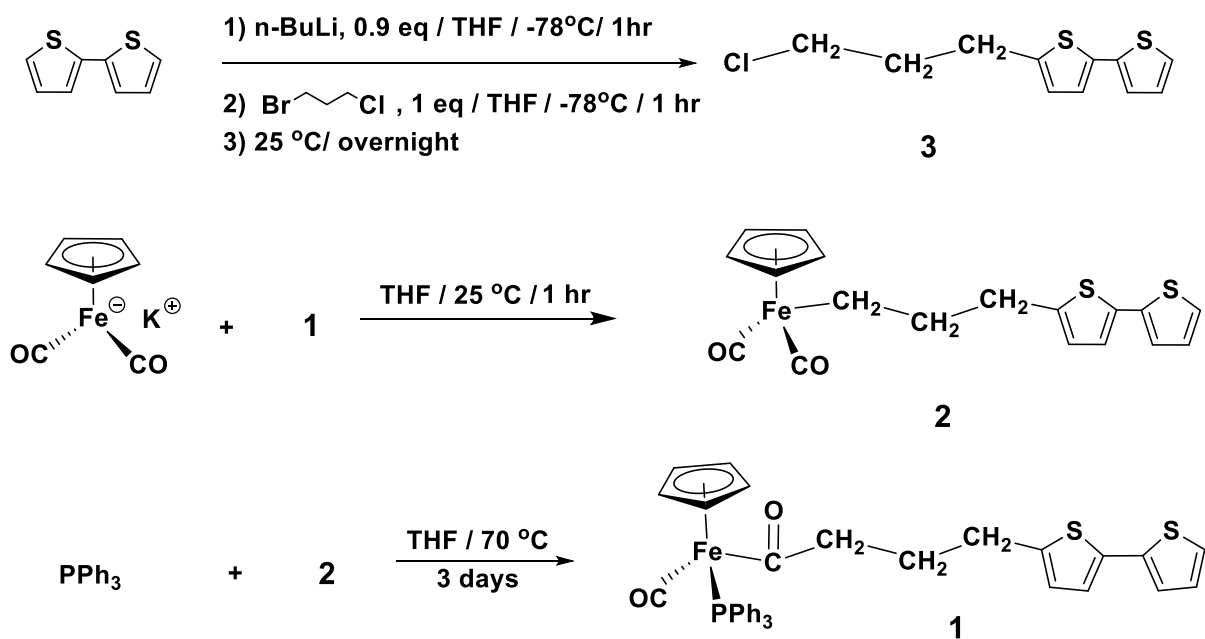
Fig. S1 ^{1}H NMR spectrum (CDCl$_3$, 25 °C, 300 MHz) of **3**.

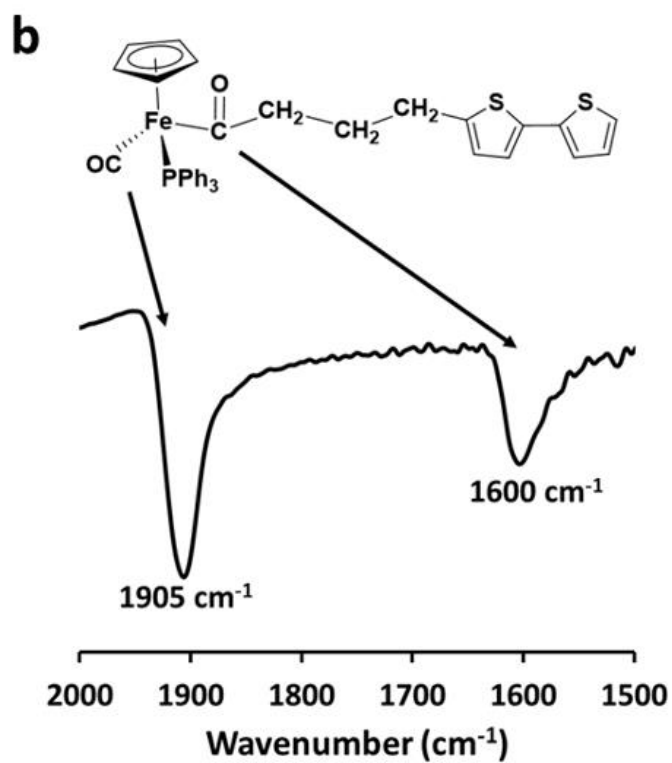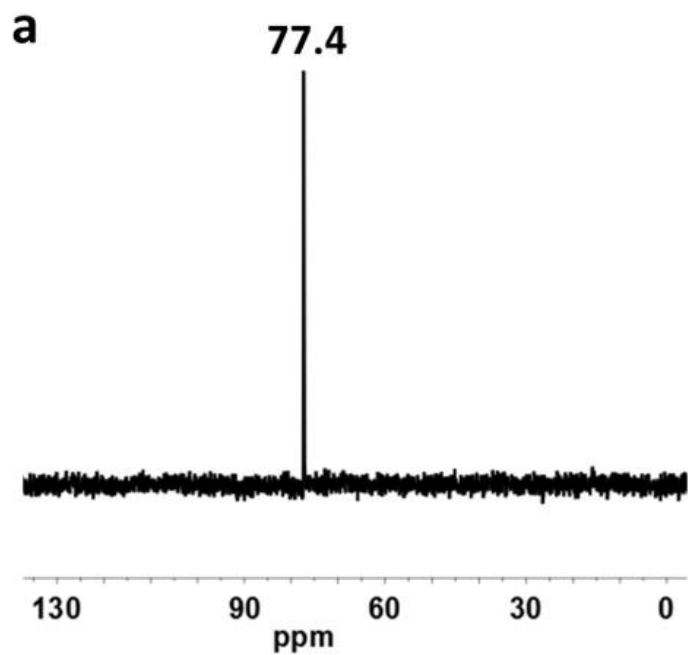**Fig. S2 (a)** ^{31}P NMR spectrum (CDCl$_3$, 25 °C, 300 MHz) of **1**; **(b)** partial FT-IR absorption spectrum (KBr pellet) for terminal and acyl CO groups from **1.**
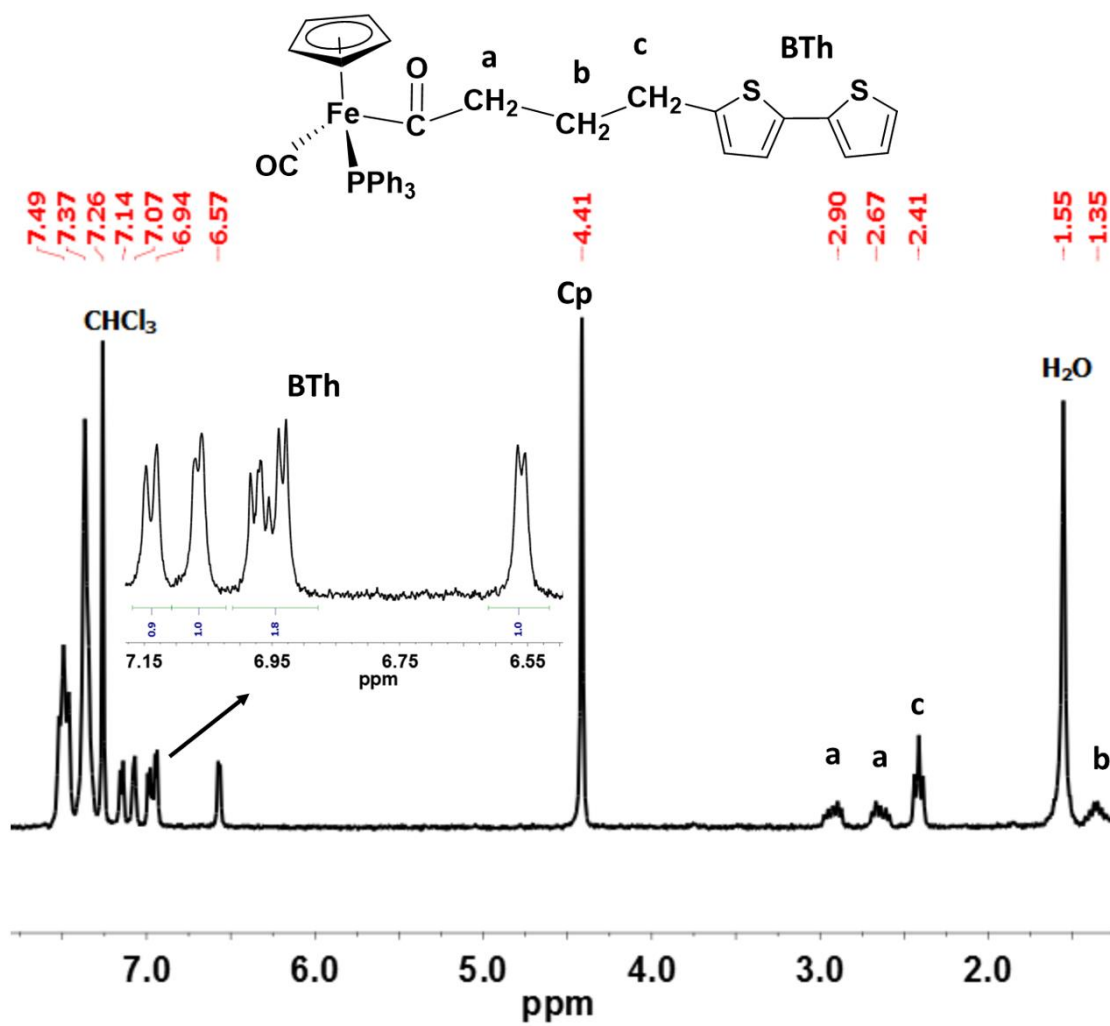
Fig. S3 ^{1}H NMR spectrum (CDCl$_3$, 25 ^{o}C, 300 MHz) of **1**.

S8

The red shift in wavenumber (Δv) for the IR absorption for both acyl and terminal CO groups of **1** in water/THF solution with water content of 80 vol% is $= 7.0$ cm^{-1} (Fig. 3 in main text)). In contrast, the terminal CO group in the non-thiophene Fp-analogue FpC6 ($\Delta v = 4.0$ cm^{-1}) is less hydrated under the same condition as we reported before.[5] This difference in the degree of hydration may influence the stability of the MC colloids. As shown in Fig. S4, DLS analysis indicated that the R_h for the colloids **1** maintained unchanged over 60 days, whereas the R_h for the FpC6 colloids gradually increased and a small amount of precipitates was observed after the sample was aged for 7 days.[5] This comparison suggests that, despite the same MC unit in the building blocks, the polarizable CO groups have varied strength of WCI.
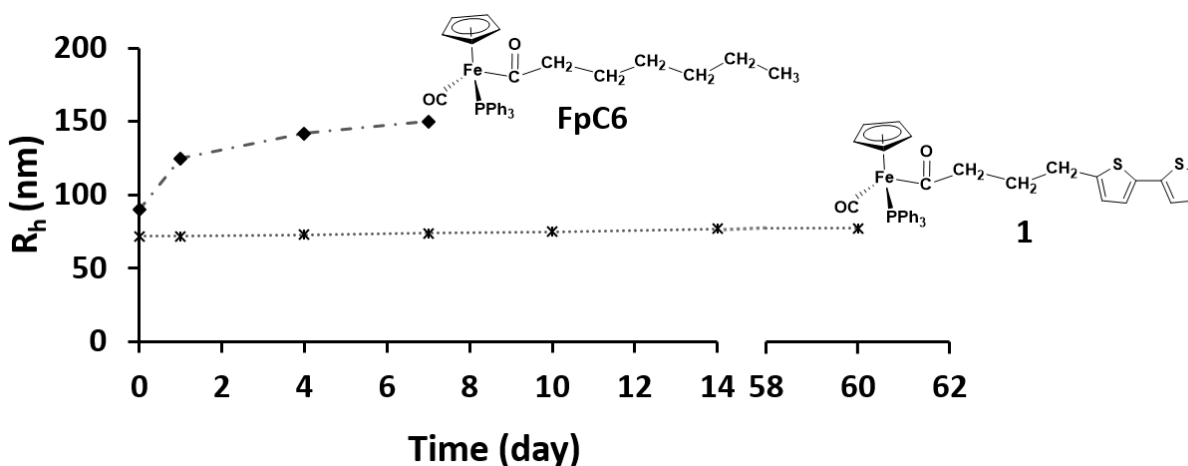

Fig. S4 Hydrodynamic radii for the aqueous colloids of **1** and FpC6 as a function of time.

[5] N. Murshid, X. Wang, *Chem. Eur. J.*, 2015, **21**, 19223 –19230
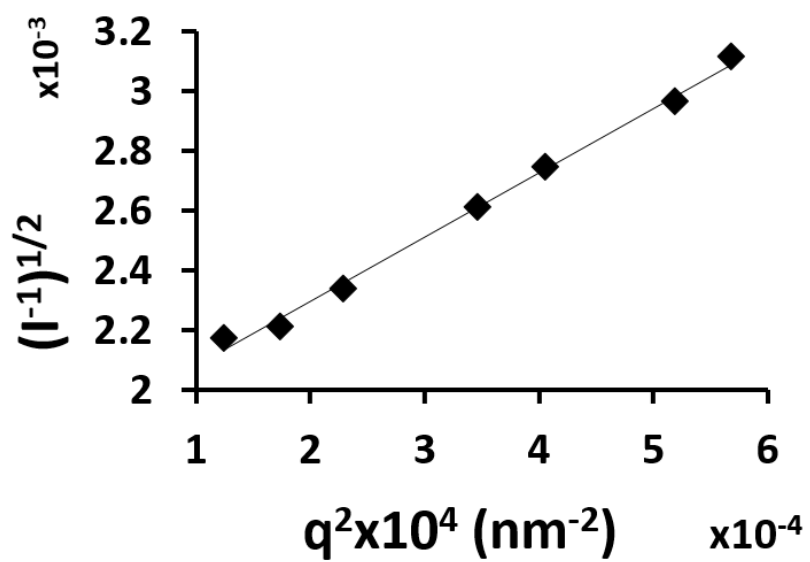
Fig. S5 Berry plot obtained from multi-angle SLS measurements of the aqueous colloids of **1** (0.77 μM)

Sample preparation methods for AFM experiments are crucial for the imaging. When the sample was prepared *via* spin coating of the colloidal solution on a freshly cleaved mica substrate, the colloids dissociated and only small fragments with vertical heights of ca. 1.0 nm were observed (Fig. S6). The observed fragments are therefore the single molecules lying on the substrates, because their heights closely match the dimension of the Fp acyl units (Fig. 5a). However, when the AFM sample prepared via drying a few drops of the solution, lamella with vertical heights of ca. 3.72 ± 0.20 nm nm were observed (Fig. S7 and 4d), which represents the membrane thickness of the broken vesicle.
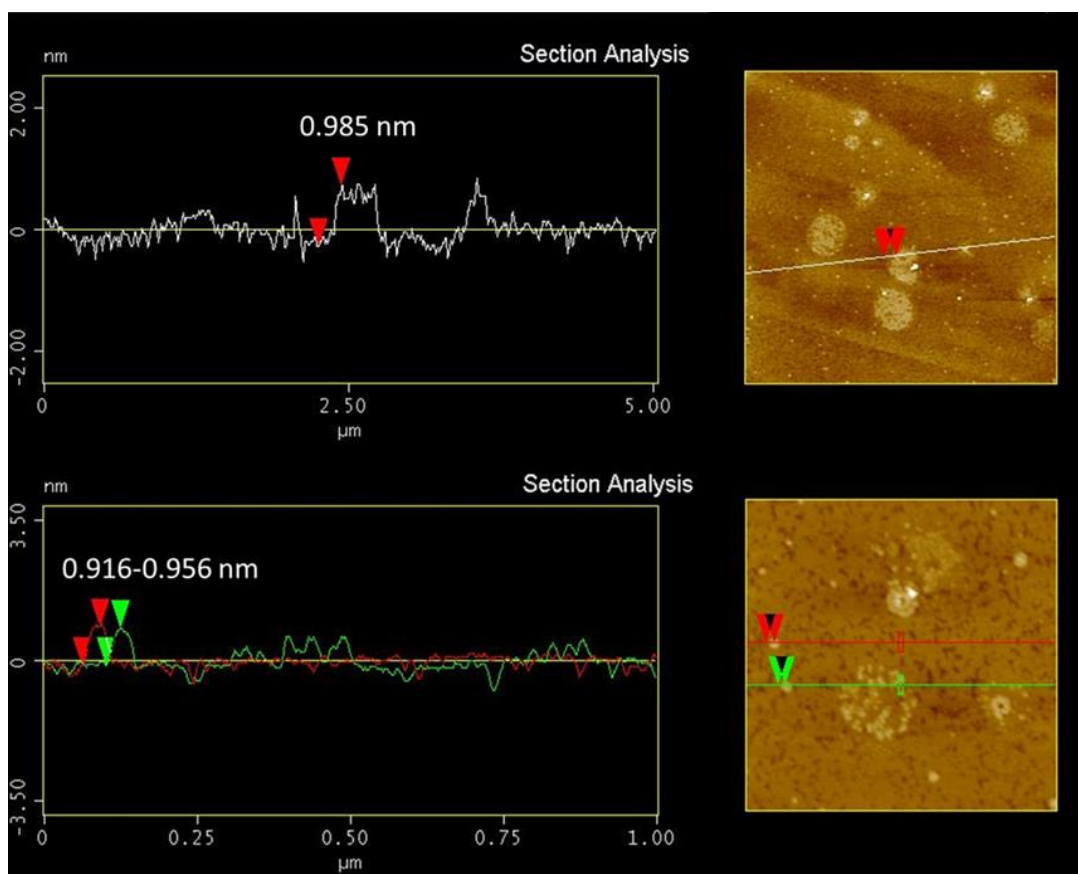

Fig. S6 Vertical section analyses of the AFM images for the sample of **1** (77 µM) prepared on mica substrates *via* spin coating.
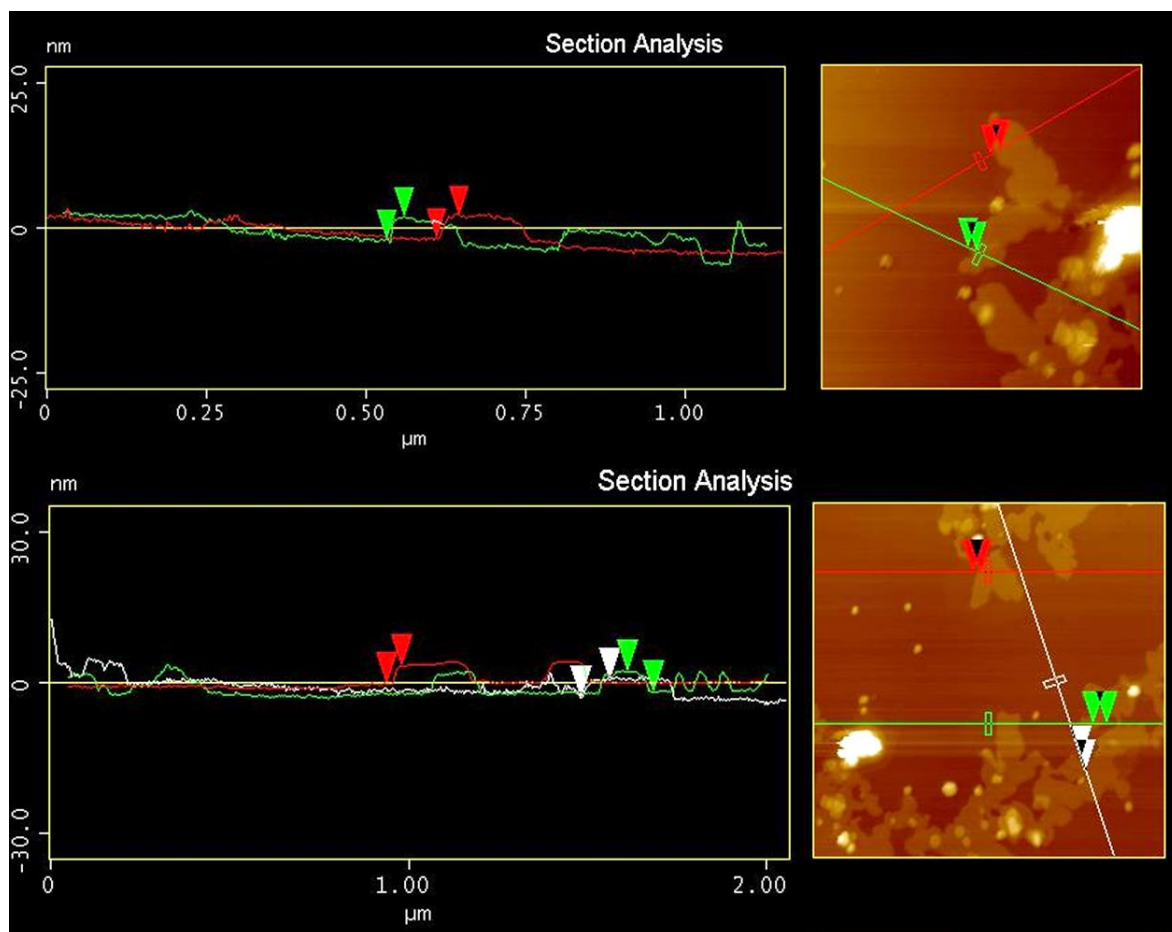
Fig. S7 Vertical section analyses of AFM images for the colloid sample of **1** (77 μM) prepared on mica substrates *via* drying a few drops of the solution.

According to the SAXS experimental results, the domain spaces 2.4 nm between the two iron centers. Cryo TEM images reveals that the thickness of the MCsome layer is ca. 3.2 nm. Accordingly, the interdigitated structure (Model 1), as shown in Figure S8a, is more possible than the non-interdigitated bilayer structure (Model 2)
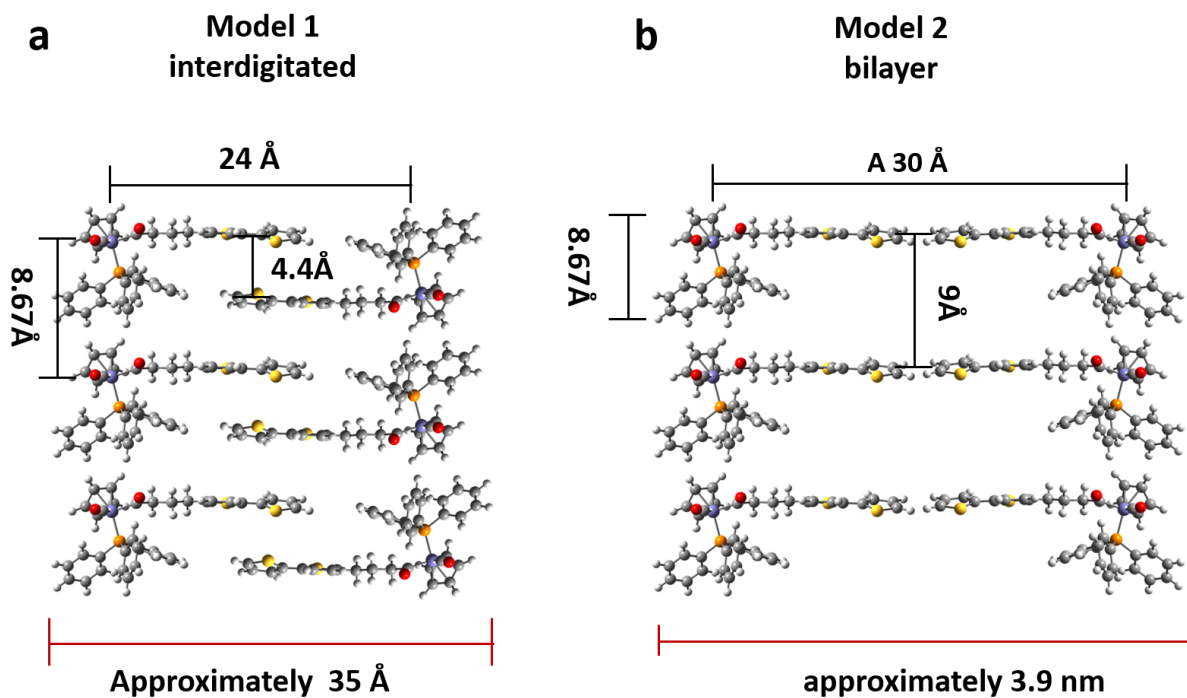

Fig. S8 (**a**) interdigitated and (**b**) non-interdigitated models for the bilayer membrane structure for the MCsome **1**.
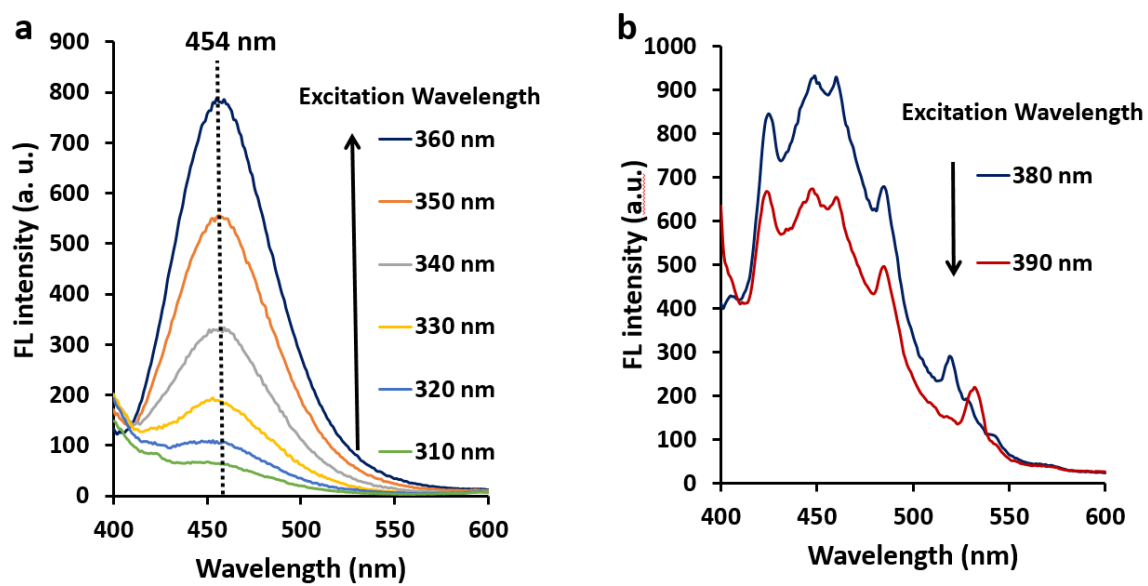
Fig. S9. FL emission spectra for the solutions of MCsome 1 in water at different excitation wavelength (λ_{ex}). The arrows represent the trend in the emission intensity with increasing λ_{ex}.
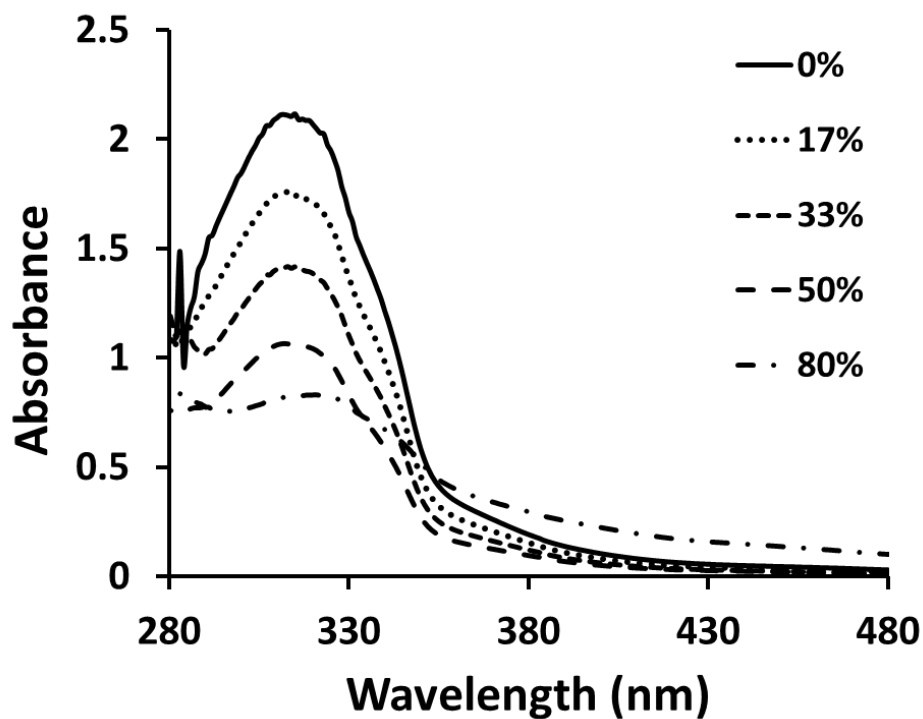
Fig. S10 UV-vis spectra for the solutions diluted from **1** in THF (154 µM) by addition of varied amounts of water.

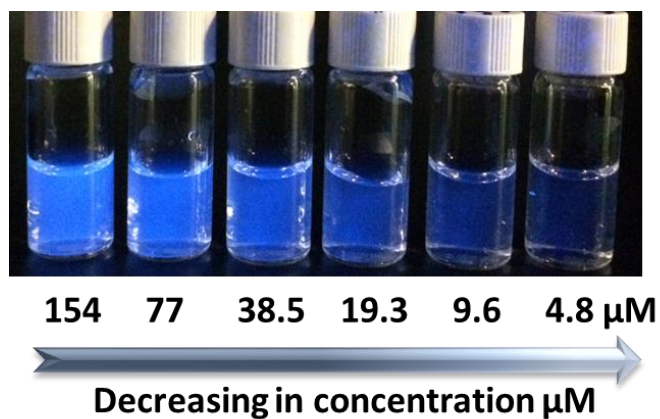**Fig. S11** Photographs for the aqueous colloids, prepared by successive dilution of the solution of **1**(154 µM), under irradiation of a UV lamb**.**

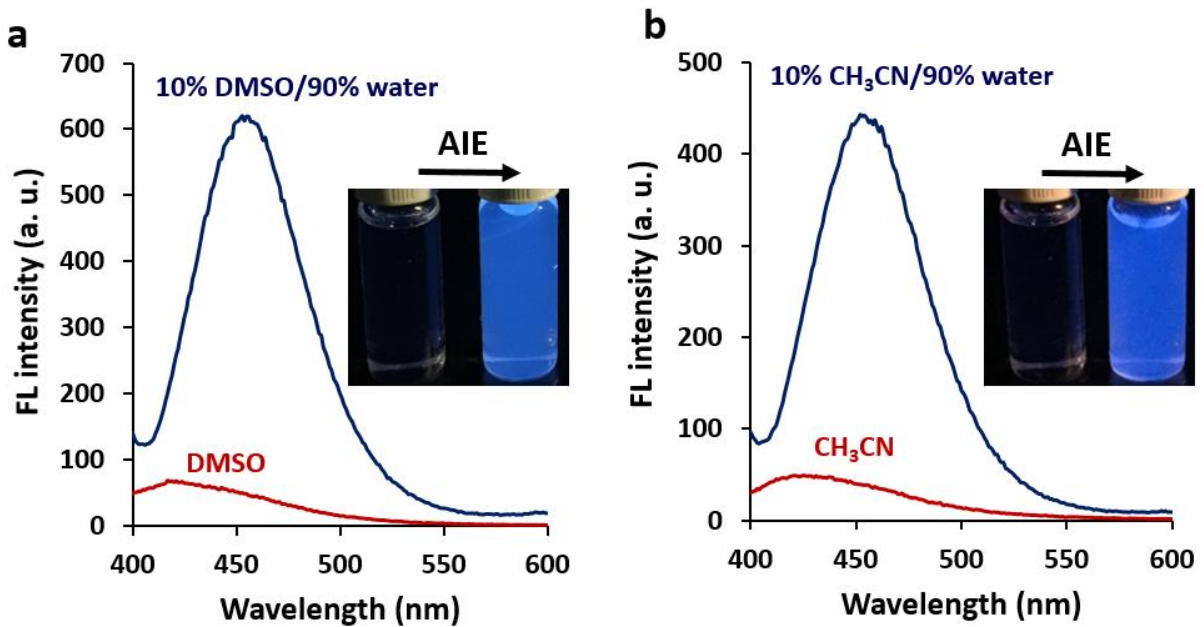**Fig. S12** FL emission spectra for the solutions of MCsome 1 in (**a**) DMSO and DMSO/water and (**b**) in acetonitrile (CH_3CN) and CH_3CN/water solutions. (λ_{ex} = 350 nm).

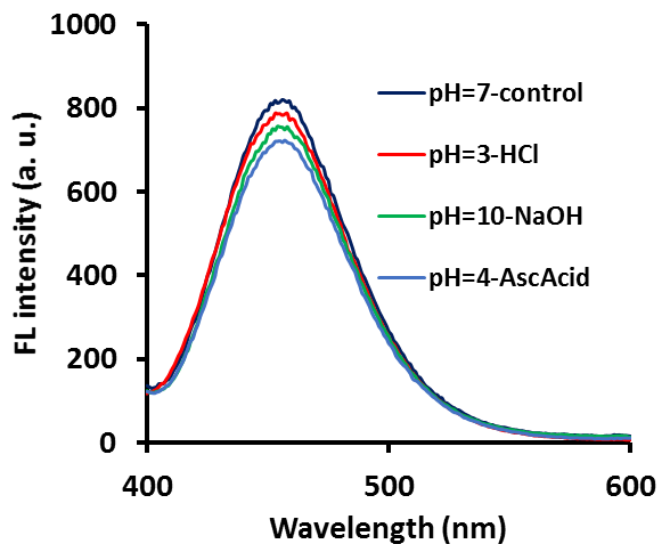**Fig. S13** FL emission spectra for the aqueous colloids of MCsome **1** at different pH. (λ_{ex}= 350 nm).

Refractive index of **1** is measured using ellipsometry. A thin film of **1** was fabricated on a silicon waver using spin coating at a medium speed. Refractive index (*n*) profile was executed from the ellipsometric data revealed from J. A. Woollam Co. VASE® ellipsometer. Data were required, at angles of incidence of 55º, 60º, 65º, 70º and 75º, with spectral range from 1700 to 400 nm. The refractive index revealed from the ellipsometric experiments is ca. 1.71 (at λ = 633 nm).
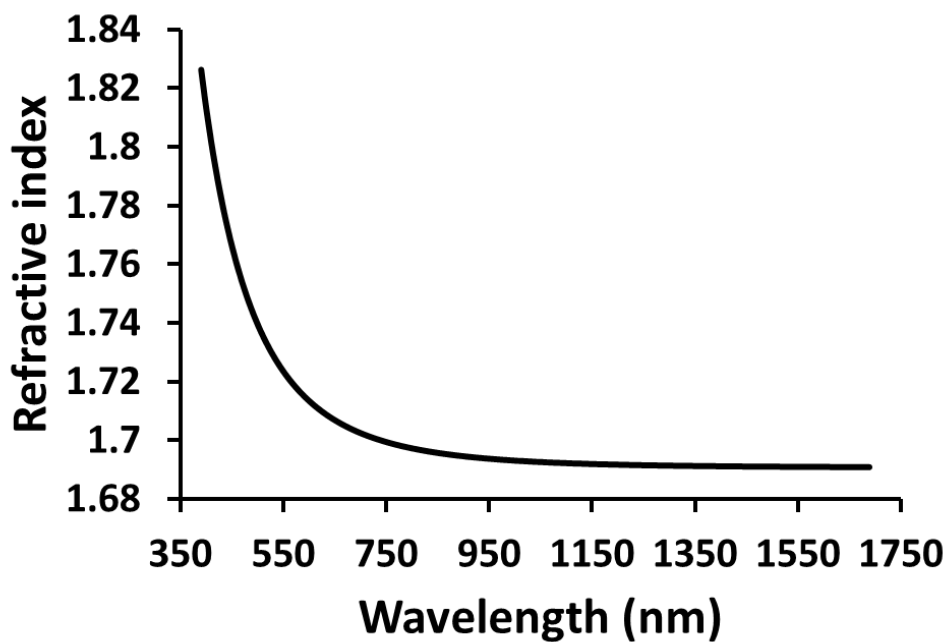

Fig. S14 Refractive index of **1** executed from the ellipsometric experiment on a spin-coated thin film of **1**.